Tellus (2005), 57B, 273–282
Printed in Singapore. All rights reserved

Copyright © Blackwell Munksgaard, 2005
TELLUS

Modelling of hydrogen and oxygen isotope compositions for local precipitation

By HAIDONG PENG[1]*, BERNHARD MAYER[2], ANN-LISE NORMAN[1] and H. ROY KROUSE[1], [1]*Department of Physics & Astronomy, University of Calgary, Calgary, Alberta, Canada T2N 1N4;* [2]*Department of Geology & Geophysics, University of Calgary, Calgary, Alberta, Canada T2N 1N4*

(Manuscript received 9 February 2004; in final form 20 January 2005)

ABSTRACT

Stable isotope compositions of hydrogen and oxygen for continental condensates are determined foremost by equilibrium and kinetic isotope fractionation during evaporation at the oceanic source regions. Subsequently they are modified by a series of in-cloud processes, which include condensation and possible admixture of vapour from evaporation and transpiration over the continents. The effects of vapour admixture from evaporation and transpiration on the isotope compositions of hydrogen (δ^2H) and oxygen (δ^{18}O) for local precipitation are discussed in this paper. Using a modified Rayleigh fractionation model, the effects are described for both constant and stepwise evaporation and transpiration fluxes. Further, deuterium (d)-excess values are employed to estimate the evaporation ratio and the slopes of δ–T polynomial regression curves are used to estimate the transpiration ratio. Finally, the influence of sea surface temperature on isotope compositions in condensates is modelled and its effect on d-excess and regression equations is examined.

1. Introduction

A fundamental physical principle in isotope hydrology is Rayleigh fractionation. This mechanism describes the evolution of isotope compositions of water vapour and condensates in an air mass during in-cloud condensation processes (e.g. Dansgaard, 1964). However, in reality, vapour recharge to a travelling air mass from evaporation and transpiration over the continent can be important. Additionally, there might be below-cloud secondary effects (secondary evaporation and isotope exchange) on raindrops. These processes are not addressed by the Rayleigh fractionation model.

Vapour recharge from continental evaporation (surface water bodies and soils) and transpiration (plants) makes up a significant portion of the atmospheric water budget (Berner and Berner, 1996). However, its contribution to local precipitation has been difficult to estimate and quantify. Isotope compositions of hydrogen and oxygen in precipitation over the continents should provide useful information in this regard.

One objective in this paper is to determine the isotope composition of in-cloud condensates. However, in most cases precipitation samples are only collected at ground level. Small samples of rain may be substantially affected by secondary evaporation and hence these samples do not represent the isotope compositions of in-cloud condensates (e.g. Dansgaard, 1964). It turns out that isotope data for snow samples and large samples of rain collected at ground level reflect those of in-cloud condensates. Solid forms of precipitation are not subject to below-cloud effects (Moser and Stichler, 1980), and secondary evaporation diminishes or ceases during events with a large amount of rain due to saturation in the air column below the cloud base. Therefore, small samples of rain are omitted when evaluating the in-cloud condensates.

In addition to the isotope characterization of in-cloud condensates, another objective of this paper is to examine how an admixture of vapour from evaporation and transpiration over the continents modifies the isotope composition of precipitation.

2. Stable isotope compositions of hydrogen and oxygen for vapour over the ocean surface

The isotope composition of hydrogen (or oxygen) in the evaporating water flux (R_E) is described by the Craig–Gordon equation (Craig and Gordon, 1965):

$$R_E = \frac{R_w - \alpha_e(T_o)h_o R_V}{\alpha^0(1-h_o)}. \quad (1)$$

The symbols are defined in the Appendix.

The isotope equilibrium fractionation factor for hydrogen or oxygen is a function of temperature (Majoube, 1971) and is denoted as $\alpha_e(T)$. T is temperature in kelvin. T_o refers to the sea surface temperature (SST). SST values are provided

*Corresponding author.
e-mail: peng@phas.ucalgary.ca

by the US National Ocean and Atmosphere Agency (NOAA; http://www.saa.noaa.gov/nsaa/products/welcome). The effects of SST on the isotope compositions of condensates will be presented later. α^0 is the kinetic fractionation factor and equals $\alpha_e(1 + \theta n C_D)$ (Gat et al., 1994). C_D is a model-dependent "kinetic constant" which relates to the molecular diffusivity of water molecules. $(C_D)_{2H} = 25‰$ and $(C_D)_{18O} = 28.5‰$ (Merlivat, 1978). n, which has values between 0 and 1, is a factor dependent on the wind regime over the water pool. The weighting factor θ ranges between 0 and 1.

The following scenario is considered: a portion f of the evaporated vapour condenses and precipitates in the atmosphere above the oceanic source region. We assume that these condensates are in isotopic equilibrium with the atmospheric water vapour. Hence, the isotope composition of hydrogen (or oxygen) for the vapour in the atmosphere above the ocean can be expressed as (Van der Straaten and Mook, 1983):

$$R_V = \frac{R_w}{\alpha(T_o)h_o + \alpha^0(1-h_o)[1-f+\alpha(T_E)f]}. \quad (2)$$

Equation (2) is the basis for further discussion. The value $f = 0.85$ is selected because more than 85% of the evaporated vapour condenses and precipitates over the ocean (Letteu, 1954; Chow, 1964). The condensation temperature T_E can be calculated using

$$T_E = \left(\frac{1}{T_o - 55} - \frac{\ln h_o}{2840}\right)^{-1} + 55$$

(Curry and Webster, 1999).

3. Modelling

The basic assumption is a "single vapour source and single air mass trajectory". An air mass acquires water vapour from a localized oceanic source and it moves to an inland station along a specific trajectory with continuous admixing of vapour fluxes from evaporation and transpiration over the continent. This admixture comprises vapour which is isotopically unfractionated by transpiration from plants (e.g. Wang and Yakir, 2000) and vapour which is isotopically fractionated by evaporation from nearby open water bodies and soils. Continental surface water is usually recharged by local precipitation either directly or by groundwater flow. Therefore, the long-term average isotope composition of precipitation at one specific site can be assumed to be equal to that of local open water bodies and soils if evaporation is minimal. Therefore, the isotope fractionation factors are related to the evaporation and transpiration fluxes, R_E and R_T, by

$$R_E = \frac{\overline{R_w} - \alpha_e h R_V}{\alpha^0(1-h)} \quad (3)$$

$$R_T = \overline{R_w}. \quad (4)$$

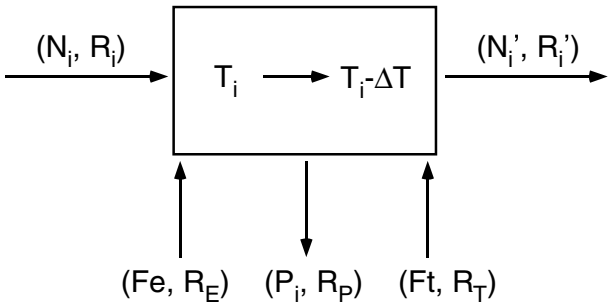

Fig. 1. Admixture of vapour in a travelling air mass with that from local evaporation and transpiration as well as the resulting condensation occurring in the atmosphere above segment L_i. The travelling air mass, with its horizontal vapour flux N_i and isotope composition R_i, enters the segment L_i (condensation temperature T_i). Here, it encounters admixture of local vapour from evaporation and transpiration. After mixing and a temperature decrease, some vapour condenses and precipitates. The remaining vapour, characterized by horizontal vapour flux N_i' and isotope composition R_i', continues to move into the next segment $i + 1$.

An air mass trajectory (denoted by L), starting from an oceanic vapour source and ending at a specific continental site, can be subdivided into a number of short segments, L_i. In-cloud condensation and admixture of moisture from evaporation and transpiration occurring in the atmosphere above a given L_i is depicted in Fig. 1. The continuity equations for vapour fluxes and their isotope compositions are:

$$N_i' - N_i = Fe + Ft - P_i \quad (5)$$

$$R_i'N_i' - R_iN_i = R_E Fe + R_T Ft - R_P P_i. \quad (6)$$

$N_i' = N_{i+1}$ and $R_i' = R_{i+1}$. N and R are the travelling vapour flux and isotope composition, respectively. The following three equations, which relate R_i to R_{i+1}, are obtained by combining eqs (3)–(6). Isotope equilibrium between condensates and water vapour in the cloud is assumed:

$$\begin{aligned} R_i' &= R_{i+1} \\ &= \frac{\frac{P_i}{N_i}\left(\frac{e_i}{\alpha^0(1-h_i)} + t_i\right)}{(\alpha_e + e_i + t_i - 1)\frac{P_i}{N_i} + 1}\overline{R_{wi}} \\ &\quad + \frac{1 - \frac{\alpha_e e_i h_i}{\alpha^0(1-h_i)}\frac{P_i}{N_i}}{(\alpha_e + e_i + t_i - 1)\frac{P_i}{N_i} + 1} R_i \end{aligned} \quad (7)$$

$$\Delta f = \frac{L}{R_w T^2}\Delta T \quad (8)$$

$$\frac{P_i}{N_i} = \frac{\Delta f}{1 - \Delta f(e_i + t_i)}. \quad (9)$$

$e_i = Fe/P_i$ and $t_i = Ft/P_i$ are the evaporation and transpiration ratios, respectively. Equations (7)–(9) constitute a

modified Rayleigh fractionation model (MRFM), which can be reduced to the classic Rayleigh fractionation model, i.e. $\Delta R = R_i - R_{i-1} = (\alpha_e - 1)R_i \Delta f$ when admixture of moisture from evaporation and transpiration is eliminated, i.e. $e_i = t_i = 0$.

Equations (7)–(9) describe the isotope evolution of water vapour in the travelling air mass, when both condensation and admixture of moisture from evaporation and transpiration are considered. These simultaneous differential equations can be solved by an iterative method. Isotope compositions of the vapour and in-cloud condensates at location L_i reflect a series of local and regional factors, which include (1) isotope compositions of atmospheric water vapour above the ocean and (2) local factors at individual sites along the air mass trajectory, such as relative humidity, condensation temperature, evaporation and transpiration ratios, isotope composition of surface waters, etc.

In solving eqs (7)–(9), it is assumed that:

(1) The oceanic vapour source lies in the subtropical trade wind belt (Peixoto and Oort, 1983). In this region, $SST_{ave} = 24.7\,^{\circ}C$ (NOAA CoastWatch Ocean Product Server: http://coastwatch.noaa.gov/interface/interface.html).

(2) The relative humidity (RH) above the ocean fluctuates between 78% ($T_E = 19.65\,^{\circ}C$) in winter and 82% ($T_E = 20.6\,^{\circ}C$) in summer.

(3) The annual average temperature at L_i is $0\,^{\circ}C$ and the average monthly temperature varies from $-15\,^{\circ}C$ (winter) to $+15\,^{\circ}C$ (summer).

(4) Evaporation and transpiration for individual sites on the air mass track are described by either constant flux for the whole year or stepwise flux, i.e. $e = t = 0$ when $T < 0\,^{\circ}C$. In contrast, $e = e_{max}$ and $t = t_{max}$ when $T > 0\,^{\circ}C$.

(5) δ^2H and $\delta^{18}O$ values for surface water at different sites follow the global meteoric water line (GMWL), i.e. $\delta^2H = 8.20\,\delta^{18}O + 11.27$, which was derived from the IAEA/WMO GNIP database (Rozanski et al., 1993).

4. Modelling results and discussion

4.1. No contribution from evaporation and transpiration

This scenario assumes continuous cooling of a travelling air mass and condensation without the admixture of continental vapour from evaporation and transpiration.

4.1.1. Correlation equation between δ^2H and $\delta^{18}O$ (local meteoric water line). The local meteoric water line (LMWL) for condensates at L_i derived from eqs (7)–(9) is $\delta^2H = 7.93\,\delta^{18}O + 8.97$, whose slope and intercept are lower than those of the GMWL. This stems solely from the temporal variation of RH values above the ocean. When this temporal variation is neglected and the RH value over the ocean surface is presumed to be temporally constant, e.g. $h = 80\%$, the LMWL at L_i is much closer to the GMWL, i.e. $\delta^2H = 8.12\,\delta^{18}O + 12.2$.

Table 1. Calculated seasonal variations of the slopes of δ^2H–T and $\delta^{18}O$–T as well as d-excess values for in-cloud condensates at site L_i, without evaporation and transpiration admixture. Continuous cooling of a travelling air mass and the subsequent condensation of its vapour are assumed. The condensation temperature is $T_e = 19.65\,^{\circ}C$ above the ocean and reaches $-15\,^{\circ}C$ at site L_i in the winter. Then it increases gradually throughout the seasons and is finally $T_e = 20.65\,^{\circ}C$ above the ocean and reaches $+15\,^{\circ}C$ at site L_i in the summer

T (°C)	$(\Delta\delta^2H/\Delta T)_0$ (‰ °C^{-1})	$(\Delta\delta^{18}O/\Delta T)_0$ (‰ °C^{-1})	d_0 (‰)
−15.0	7.33	0.91	10.70
−13.5	7.17	0.89	10.60
−12.0	7.01	0.88	10.50
−10.5	6.85	0.86	10.43
−9.0	6.69	0.84	10.37
−7.5	6.54	0.82	10.33
−6.0	6.38	0.80	10.30
−4.5	6.23	0.79	10.27
−3.0	6.08	0.77	10.23
−1.5	5.93	0.75	10.19
0.0	5.78	0.73	10.15
1.5	5.64	0.71	10.10
3.0	5.49	0.70	10.04
4.5	5.35	0.68	9.96
6.0	5.21	0.66	9.87
7.5	5.08	0.64	9.76
9.0	4.94	0.62	9.64
10.5	4.81	0.61	9.48
12.0	4.68	0.59	9.31
13.5	4.55	0.57	9.11
15.0	4.52	0.55	8.88

4.1.2. Correlation equations between δ values and temperature. The calculated linear temperature dependences of δ^2H and $\delta^{18}O$ values for condensates at L_i are $\delta^2H = 5.81T - 107.63$ and $\delta^{18}O = 0.72T - 14.72$, respectively. However, the slope of the δ–T relationship deserves more attention. In many cases, δ values exhibit a quadratic relationship with T, and hence a polynomial regression provides a better correlation between δ and temperature values. By solving eqs (7)–(9), the quadratic relationships between δ^2H–T and $\delta^{18}O$–T at L_i were found to be $\delta^2H = -0.048T^2 + 5.88T - 112.45$ and $\delta^{18}O = -0.006T^2 + 0.73T - 15.34$, respectively. Table 1 shows the dependence of calculated $\Delta\delta/\Delta T$ values with local temperature. For example, the $\Delta\delta^2H/\Delta T$ value decreases from 7.47‰ °C^{-1} ($T = -15\,^{\circ}C$) to 4.59‰ °C^{-1} ($T = -15\,^{\circ}C$).

4.1.3. Deuterium (d)-excess values. d-excess is defined as

$$\text{d-excess} = \delta^2H - 8\,\delta^{18}O.$$

It is common to observe higher d-excess values for winter precipitation than in summer at sites with precipitation from a single oceanic vapour source (Rozanski et al., 1993). This seasonality

of d-excess values is attributed to three mechanisms: (1) lower relative humidity over the source region in winter than in summer (e.g. Merlivat and Jouzel, 1979); (2) snow formation processes (Jouzel and Merlivat, 1984) and (3) secondary evaporation of rain drops during their descent from the cloud base to the ground (e.g. Dansgaard, 1964).

Table 1 shows the seasonal variation of calculated d-excess values for in-cloud condensates at L_i due to seasonality of RH over the ocean. d-excess values decrease from 10.70‰ (h_o = 78%) in winter to 8.88‰ (h_o = 82‰) in summer. Hence, sites with precipitation dominated by oceanic vapour generally have decreasing d-excess values with increasing local temperature (Schotterer et al., 1993). Moreover, d-excess values at L_i were expected to increase further in winter above 10.70‰ due to snow formation and to decrease further in summer below 8.88‰ due to secondary evaporation.

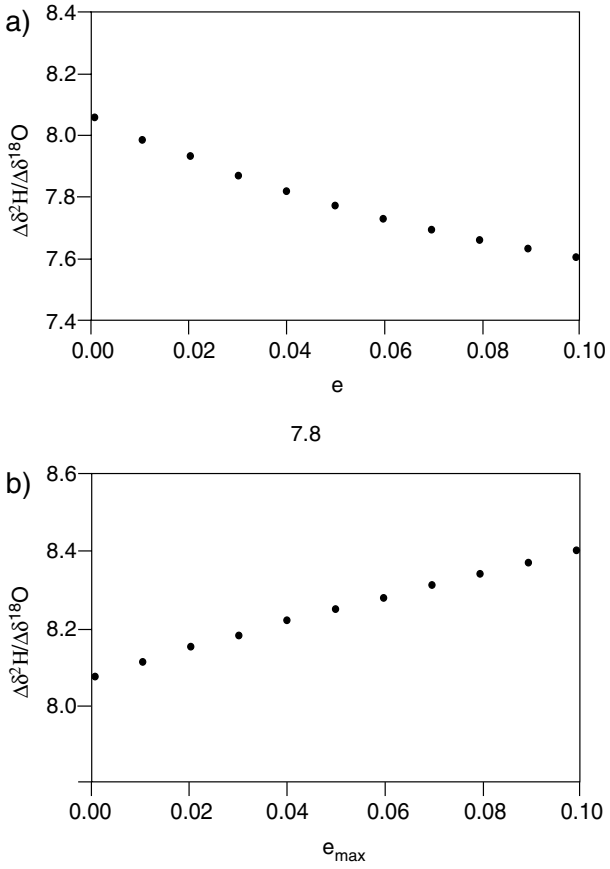

Fig. 2. Dependence of the calculated slopes of LMWL ($\Delta\delta^2$H/$\Delta\delta^{18}$O) for condensates at site L_i on the evaporation ratios (eqs 7–9), for constant flux (a) and a stepwise flux scheme (b). Evaporative moisture decreases (constant flux) or increases (stepwise flux) the slope of δ^2H–δ^{18}O, compared with the non-evaporative scenario ($e = 0$ or $e_{max} = 0$). Also, $\Delta\delta^2$H/$\Delta\delta^{18}$O tends to decrease further (constant flux) or increase (stepwise flux) with increasing evaporation ratio.

Table 2. Use of eq. (10) to estimate the evaporation ratios. With a given evaporation ratio of $e = 5\%$ (constant flux) or $e_{max} = 5\%$ (stepwise flux), the temperature dependence of d-excess values for condensates at site L_i were calculated from eqs (7)–(9), as shown in columns 4 and 6. Then the results were substituted into eq. (10) to calculate f_e, as shown in column 5 and column 7. In both cases, "f_e" was close to "e" or "e_{max}", which suggests that this simplified method is consistent with the modified Rayleigh fractionation model (MRFM) and could be used in the future to estimate evaporation ratios. Column 2 is identical to column 4 in Table 1. Column 3 is derived from eq. (11)

			$e = 5\%$		$e_{max} = 5\%$	
T (°C)	d_0 (‰)	d_e (‰)	d (‰)	f_e (%)	d (‰)	f_e (%)
−15.0	10.70	96.30	15.20	5.20	10.70	0.00
−13.5	10.60	96.20	15.00	5.10	10.60	0.00
−12.0	10.50	96.10	15.00	5.20	10.50	0.00
−10.5	10.43	96.00	14.80	5.10	10.43	0.00
−9.0	10.37	96.00	14.80	5.20	10.37	0.00
−7.5	10.33	95.90	14.70	5.10	10.33	0.00
−6.0	10.30	95.90	14.70	5.10	10.30	0.00
−4.5	10.27	95.90	14.60	5.10	10.27	0.00
−3.0	10.23	95.80	14.60	5.10	10.23	0.00
−1.5	10.19	95.80	14.60	5.10	10.19	0.00
0.0	10.15	95.80	14.50	5.10	10.15	0.00
1.5	10.10	95.70	14.50	5.10	14.50	5.10
3.0	10.04	95.60	14.40	5.10	14.30	5.00
4.5	9.96	95.60	14.30	5.10	14.20	5.00
6.0	9.87	95.50	14.30	5.20	14.20	5.00
7.5	9.76	95.40	14.30	5.30	14.00	5.00
9.0	9.64	95.20	14.20	5.30	14.00	5.10
10.5	9.48	95.10	13.90	5.20	13.80	5.00
12.0	9.31	94.90	13.80	5.30	13.70	5.10
13.5	9.11	94.70	13.40	5.00	13.50	5.10
15.0	8.88	94.50	13.20	5.10	13.30	5.20

4.2. *The contribution of vapour from evaporation*

4.2.1. Dependence of the correlation between δ^2H and $\delta^{18}O$ values (LMWL) on continental evaporation admixture. Figure 2 shows the relationship of calculated slopes of δ^2H–δ^{18}O ($\Delta\delta^2$H/$\Delta\delta^{18}$O) at L_i versus evaporation ratios for both constant and stepwise fluxes. Evaporation vapour either decreases (constant flux) or increases (stepwise flux) the $\Delta\delta^2$H/$\Delta\delta^{18}$O values, compared with the non-evaporative scenario ($e = 0$ or $e_{max} = 0$). Also, $\Delta\delta^2$H/$\Delta\delta^{18}$O values further decrease (constant flux) or increase (stepwise flux) with increasing evaporation ratios. The reasons are as follows: admixture of evaporative flux increases the d-excess value of atmospheric moisture. Also, d_{evap} demonstrates an inverse relationship with local temperature (Table 2). Hence, for a constant flux, evaporative flux increases the d-excess values for vapour and condensates by different degrees in different seasons: maximum in winter and minimum in summer. This results in a decrease of the δ^2H–δ^{18}O slope. On the other hand, for the stepwise flux scheme, evaporative flux increases

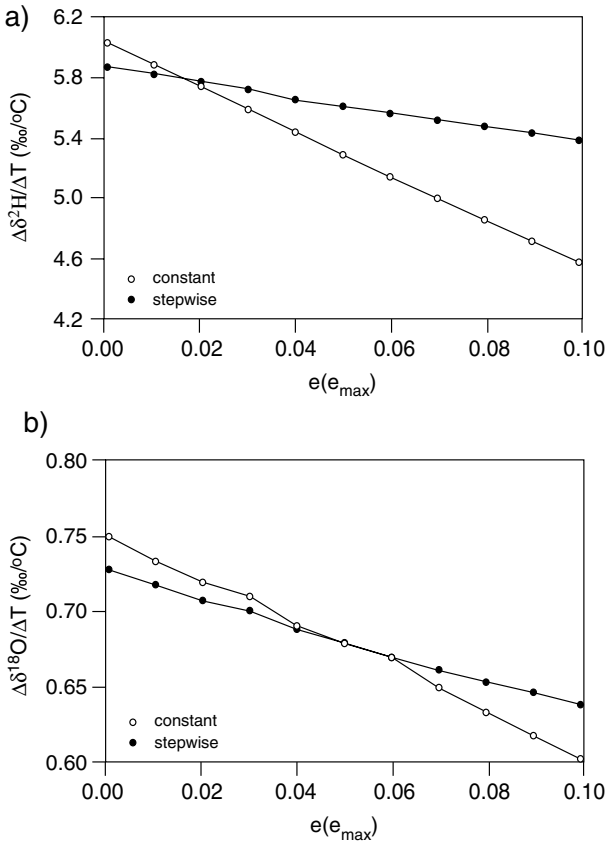

Fig. 3. Dependence of the calculated slopes of δ–T (δ^2H–T and δ^{18}O–T) for condensates at site L_i on the evaporation ratios (eqs 7–9), for both evaporation schemes. In both scenarios, evaporative moisture flux tends to decrease the slope of δ–T correlation line compared with the non-evaporation scenario ($e = 0$ and $e_{\max} = 0$). Also, the slope of δ–T tends to further decrease with increasing evaporation ratio.

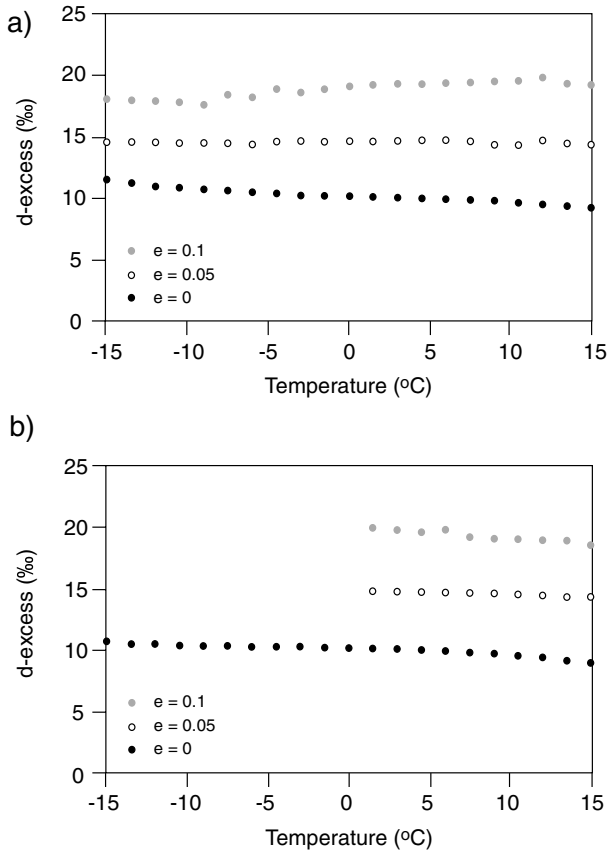

Fig. 4. Dependence of calculated d-excess values for condensates at site L_i on the evaporation ratios (eqs 7–9), for both evaporation schemes. In both schemes, a marked increase of d-excess values for condensates at site L_i, compared with the non-evaporation scenario, is observed.

the d-excess value of condensates only at $T > 0\,^{\circ}$C, which leads to an increase of the δ^2H–δ^{18}O slope.

4.2.2. Dependence of correlation between δ values and temperatures on the continental evaporation admixture. Figure 3 shows the relationship of calculated slopes of δ^2H–T and δ^{18}O–T versus evaporation ratios, for both constant and stepwise flux schemes. In both cases the evaporation flux decreases the slope of the δ–T relationship. Surface water and soil water with long residence times have almost constant isotope compositions and thus it is reasonable to assume that no correlation exists between the δ values for evaporation flux and local temperature. Therefore, after mixing with the evaporation flux of zero δ–T slope, the atmospheric vapour and condensates are characterized by lower δ–T slopes than the advecting vapour from the ocean.

4.2.3. Dependence of d-excess values on continental evaporation admixture. Figure 4 depicts the relationship of d-excess values for condensates at L_i versus evaporation ratios. In both constant and stepwise flux schemes, d-excess values increase due to the admixture of the evaporated moisture compared with the non-evaporation scenario. Moreover, d-excess values increase with increasing evaporation ratios "e" (constant flux) or "$e_{\max}$" (stepwise flux). The variation of d-excess values for atmospheric vapour and the subsequent condensates caused by the admixture of evaporation flux has been addressed by several authors (Gat and Matsui, 1991; Ingraham and Taylor, 1991; Gat et al., 1994). Evaporation moisture usually has higher d-excess values than the incoming advection moisture. Hence, mixing of these two moisture fluxes results in a higher d-excess value compared with the advection moisture. This could explain the observation that d-excess values of precipitation in Mongolia were elevated with increasing temperatures (Schotterer et al., 1993).

4.2.4. Estimation of continental vapour admixture to precipitation using d-excess values. Until now, a range of known evaporation ratios has been used to calculate d-excess values for condensates at L_i. However, the reverse procedure, i.e. estimating the contribution of continental evaporation from the known d-excess values of condensates at L_i, is more practical. Therefore, a simplified method to employ d-excess values as a diagnostic tool

to quantify the vapour contribution from regional evaporation to local precipitation is suggested. The principle is as follows: the d-excess value for local condensates is assumed to have two components, a fraction f_e derived from continental evaporation flux (d_{evap}) and a fraction of $1 - f_e$ from advection vapour (d_{adv}). Thus $d = (1 - f_e)d_{adv} + f_e d_{evap}$. Hence, the continental evaporation ratios can be estimated as

$$f_e = \frac{d - d_{adv}}{d_{evap} - d_{adv}}. \quad (10)$$

The d-excess value of moisture from continental evaporation was calculated (Gat et al., 1994) as follows:

$$d_{evap} = \frac{d_{surf} - d_{adv}}{1 - h} + 107\theta + d_{adv}. \quad (11)$$

It is essential to test if this over-simplified practice is consistent with the MRFM in eqs (7)–(9) and therefore whether this method can provide a reasonable estimate of evaporation ratios. Here, a "loop" technique is employed: (1) with a given evaporation ratio, d-excess values for condensates at L_i were calculated from eqs (7)–(9); (2) these results were then substituted into eq. (10) to calculate f_e.

Table 2 summarizes the results for both constant and stepwise evaporation flux scenarios. It is apparent that f_e is close to "e" (constant flux) or "e_{max}" (stepwise flux). Hence, this simplified method is consistent with the MRFM and it is suggested that it could be employed to estimate the continental evaporative ratio, to a first-order approximation.

4.3. The contribution of vapour from transpiration

4.3.1. Dependence of relationship between δ^2H and $\delta^{18}O$ values on transpiration ratio. Calculations from eqs (7)–(9) show no apparent dependence between slopes of δ^2H–δ^{18}O ($\Delta\delta^2$H/$\Delta\delta^{18}$O) and transpiration ratios, for both constant flux and stepwise flux schemes. The isotope compositions of transpiration vapour are identical to those of long-term local precipitation so that the admixture of transpiration vapour does not appreciably affect the local δ^2H–δ^{18}O relationship.

4.3.2. Dependence of δ values versus temperatures on the transpiration ratio. Figure 5 shows the relationship of calculated slopes of δ^2H–T($\Delta\delta^2$H/ΔT) and δ^{18}O–T($\Delta\delta^{18}$O/ΔT) for condensates versus transpiration ratios for both constant and stepwise flux schemes. For constant flux, $\Delta\delta^2$H/ΔT decreases monotonically with increasing transpiration ratio. Plants usually transpire soil moisture with δ values close to that of mean annual precipitation and little or no correlation exists between δ values and the local temperature. Therefore, after mixing with the transpiration vapour of near zero δ–T slopes, the integrated vapour and the subsequent condensates show lower slopes of δ–T than the advecting vapour originating from the oceans. Moreover, the slopes of δ–T decrease further with increasing transpiration ratio.

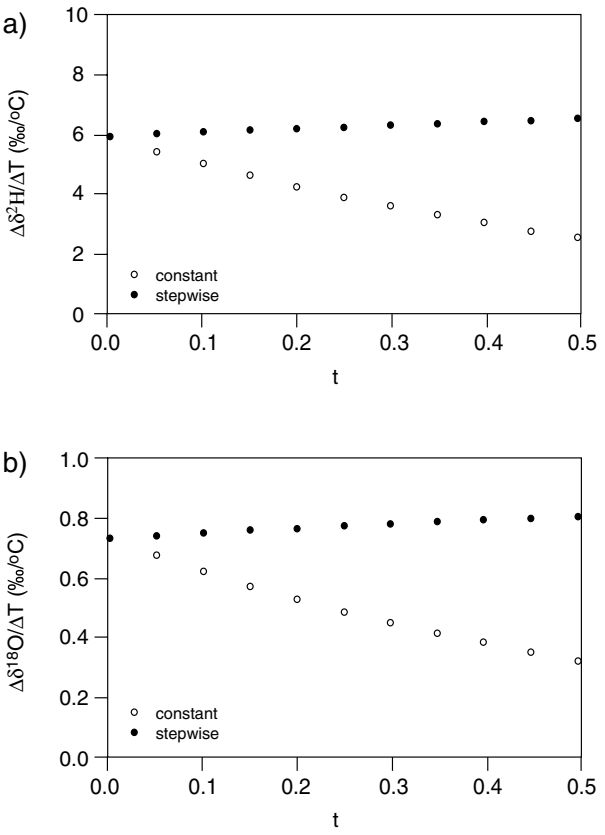

Fig. 5. The dependence of $\Delta\delta^2$H/ΔT and $\Delta\delta^{18}$O/ΔT values for condensates at site L_i on transpiration ratios.

However, with stepwise flux, $\Delta\delta^2$H/ΔT and $\Delta\delta^{18}$O/ΔT increases monotonically with increasing transpiration ratio. In this scheme, δ values of the condensates below 0 °C remain unchanged because of the absence of transpiration vapour. In contrast, the δ values of condensates above 0 °C increase beyond those of the non-transpiration case due to the admixture of vapour from continental transpiration. Without isotope fractionation, the transpiration vapour fluxes have higher δ values than those of advecting vapour. Thus, after mixing, the vapour and the resulting condensates have higher δ values, reflecting the isotope composition of surface waters. Therefore the temporal amplitude of δ–T curves is amplified and the slope of the δ–T correlation equation tends to increase. It is apparent that this increase will be more pronounced with increasing transpiration ratios (Hoffmann et al., 2000).

Despite the different patterns of the δ–T slopes for condensates for different transpiration schemes, a common characteristic for δ–T polynomial regression curves is apparent in both cases: the slopes decrease monotonically with increasing temperature. Figure 6 shows the relationship between $\Delta\delta^2$H/ΔT and temperature T for constant transpiration flux (Fig. 6a) and stepwise transpiration flux (Fig. 6b) scenarios. In both schemes, it is shown

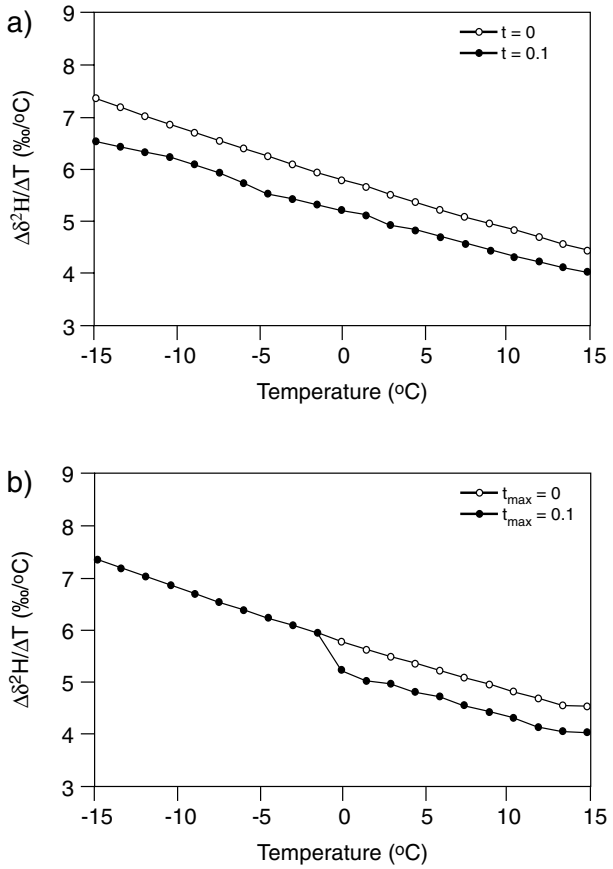

Fig. 6. Dependence of the slopes of δ^2H–T regression curves ($\Delta\delta^2\mathrm{H}/\Delta T$) for condensates on temperature, for constant flux (a) and stepwise flux (b) schemes. In both cases, the slope decreases monotonically with increasing temperature.

that the slopes decrease monotonically with increasing temperatures.

4.3.3. Estimation of transpiration admixture to precipitation using δ–T slopes. Analogous to the above calculation for evaporation flux, a simplified method to employ the slopes of the δ–T regression curves as diagnostic tools to quantify the vapour contribution from transpiration to local precipitation is suggested. The principle is as follows: the δ value for local condensates is assumed to have two components—a fraction f_t from transpiration flux (δ_{transp}) and a fraction, $1 - f_t$, coming from the advecting vapour flux (δ_{adv}). Thus $(1 - f_t)\delta_{\mathrm{adv}} + f_t\delta_{\mathrm{transp}} = \delta_{\mathrm{precip}}$.

Assuming $(\Delta\delta/\Delta T)_{\mathrm{transp}} = 0$, the continental transpiration ratios can be estimated by:

$$f_t = \frac{(\Delta\delta/\Delta T)_{\mathrm{adv}} - (\Delta\delta/\Delta T)_{\mathrm{precip}}}{(\Delta\delta/\Delta T)_{\mathrm{adv}}}. \quad (12)$$

It is essential to test if this over-simplified procedure is consistent with the MRFM and therefore whether this method can provide a reasonable estimate of transpiration ratios. Here, a "loop" technique is employed: (1) with a given transpiration ratio, $\Delta\delta/\Delta T$ values for condensates at L_i were calculated from eqs. (7)–(9); (2) these results were then substituted into eq. (12) to calculate f_t.

Table 3. Use of eq. (12) to estimate the transpiration ratios. With a given evaporation ratio of $t = 10\%$ (constant flux) or $t_{\max} = 10\%$ (stepwise flux), the temperature dependence of $(\Delta\delta^2\mathrm{H}/\Delta T)_{\mathrm{condensates}}$ values for condensates at site L_i were calculated using eqs. (7)–(9), as shown in columns 3 and 5. Then the results were substituted into eq. (12) to calculate f_t, as shown in columns 4 and 6. In both cases, "f_t" is close to "t" or "$t_{\max}$", which suggests that this simplified method is consistent with the modified Rayleigh fractionation model (MRFM) and could be used in the future to estimate transpiration ratios. Column 2 is identical to column 2 in Table 1

	$t = 0$	$t = 10\%$		$t_{\max} = 10\%$	
T (°C)	$(\Delta\delta^2\mathrm{H}/\Delta T)_0$ (‰ °C^{-1})	$\Delta\delta^2\mathrm{H}/\Delta T$ (‰ °C^{-1})	f_t (%)	$\Delta\delta^2\mathrm{H}/\Delta T$ (‰ °C^{-1})	f_t (%)
−15.0	7.33	6.50	11.3	7.33	0.0
−13.5	7.17	6.40	10.7	7.17	0.0
−12.0	7.01	6.30	10.1	7.01	0.0
−10.5	6.85	6.20	9.5	6.85	0.0
−9.0	6.69	6.07	9.3	6.69	0.0
−7.5	6.54	5.90	9.8	6.54	0.0
−6.0	6.38	5.70	10.7	6.38	0.0
−4.5	6.23	5.50	11.7	6.23	0.0
−3.0	6.08	5.40	11.2	6.08	0.0
−1.5	5.93	5.30	10.6	5.93	0.0
0.0	5.78	5.20	10.1	5.22	9.8
1.5	5.64	5.10	9.5	5.02	10.9
3.0	5.49	4.90	10.8	4.97	9.6
4.5	5.35	4.80	10.3	4.81	10.2
6.0	5.21	4.63	11.2	4.73	9.3
7.5	5.08	4.55	10.3	4.55	10.3
9.0	4.94	4.48	9.4	4.42	10.6
10.5	4.81	4.30	10.6	4.31	10.3
12.0	4.68	4.20	10.3	4.13	11.7
13.5	4.55	4.10	10.0	4.06	10.9
15.0	4.52	4.00	10.9	4.01	11.3

Table 3 summarizes the results for both constant and stepwise flux scenarios. It is apparent that f_t is close to "t" (constant flux) or "$t_{\max}$" (stepwise flux). Hence, this simplified method is consistent with the MRFM and it is suggested that it could be employed to estimate transpiration ratios to a first-order approximation (Jacob and Sonntag, 1991).

4.3.4. Dependence of d-excess values on the transpiration ratio. From the MRFM, it is apparent that there is no marked variation of d-excess values due to the admixture of transpiration vapour. Because transpiration vapour is not isotopically fractionated relative to soil water, the d-excess values of the atmospheric vapour and the resultant condensates remain unchanged (Salati et al., 1979).

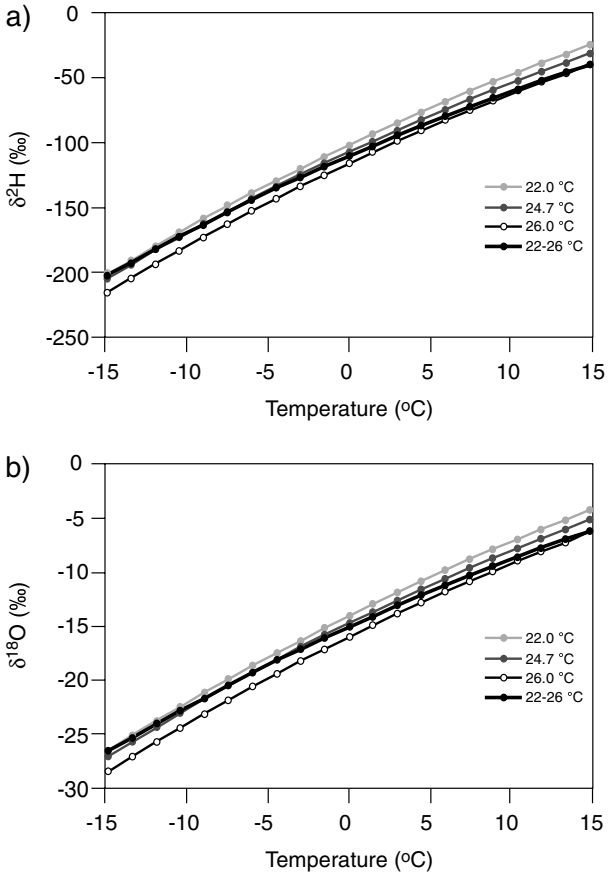

Fig. 7. Four scenarios of the dependence of isotope compositions of hydrogen and oxygen on SST: SST = 22 °C; SST = 24.7 °C; SST = 26 °C and SST varying from 22 °C in the winter to 26 °C in the summer. Isotope compositions for condensates at site L_i decrease with increasing SST values. The ranges of decrease are seasonally different, i.e. smallest in winter and largest in summer.

4.4. The influence of sea surface temperature (SST)

Variations in isotope compositions of local condensates caused by changes in SST at the oceanic source region were also examined. The hypothetical continental site L_i was chosen for discussion. Four SST scenarios were selected: SST = 22 °C; SST = 24.7 °C; SST = 26 °C and SST varying from 22 °C in the winter to 26 °C in the summer.

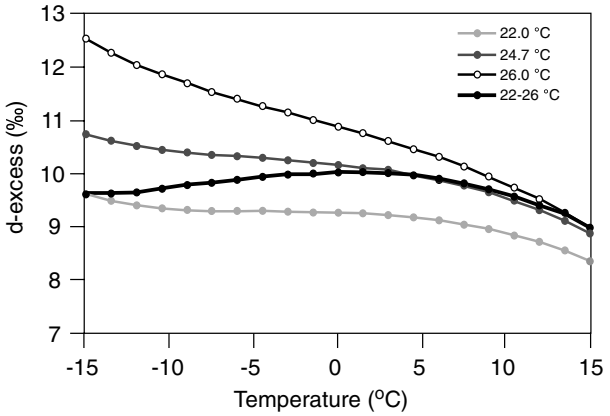

Fig. 8. Four scenarios of the dependence of d-excess values on SST: SST = 22 °C; SST = 24.7 °C; SST = 26 °C and SST varying from 22 °C in the winter to 26 °C in the summer. d-excess for continental precipitation increases with increasing SST. The ranges of increase vary seasonally, being largest in winter and smallest in summer.

4.4.1. Dependence of δ^2H, $\delta^{18}O$, δ^2H–T and $\delta^{18}O$–T correlations on SST. Figure 7 shows the variation of δ^2H and δ^{18}O values with SST. It is apparent that isotope compositions for condensates at L_i decrease with increasing SST values. The extent of the decrease at L_i is different for different seasons, i.e. smallest in the winter and largest in the summer (3.15‰ °C^{-1} and 0.48‰ °C^{-1} for δ^2H and δ^{18}O in the winter and 3.78‰ °C^{-1} and 0.49‰ °C^{-1} in the summer). This characteristic determines the decrease of δ^2H–T and δ^{18}O–T slopes with increase in SST. Table 4 shows the variations of δ^2H–T and δ^{18}O–T regression lines for different SST scenarios (about 0.023° C^{-1} for δ^2H–T and about 7.5 × 10^{-3} ° C^{-1} for δ^{18}O–T). This result suggests that using simplified models to estimate palaeotemperatures at a continental site may be problematic. It is interesting that in the fourth scenario (SST varies from 22 °C in the winter to 26 °C in the summer at the oceanic source region), isotope compositions for condensates at L_i have the highest *winter* value and the lowest *summer* values, compared with the first three scenarios, which indicates the lowest δ^2H–T and δ^{18}O–T slope.

4.4.2. Dependence of d-excess values and δ^2H–$\delta^{18}O$ correlation on SST. Variations of d-excess values with SST are shown in Fig. 8. d-excess is expected to increase with increasing SST, although the ranges vary for different seasons, i.e. highest in the

Table 4. The variations of δ^2H–δ^{18}O, δ^2H–T and δ^{18}O–T regression lines according to four different SST scenarios, i.e. SST = 22 °C; SST = 24.7 °C; SST = 26 °C and SST varies from 22 °C in winter to 26 °C in summer

SST (°C)	δ^2H–δ^{18}O	δ^2H–T	δ^{18}O–T
22	$\delta^2H = 8.10\delta^{18}O + 10.66$	$\delta^2H = 5.94T - 106.83$	$\delta^{18}O = 0.735T - 14.50$
24.7	$\delta^2H = 8.03\delta^{18}O + 10.70$	$\delta^2H = 5.88T - 116.43$	$\delta^{18}O = 0.734T - 15.84$
26	$\delta^2H = 7.99\delta^{18}O + 10.74$	$\delta^2H = 5.85T - 120.81$	$\delta^{18}O = 0.732T - 16.45$
22–26	$\delta^2H = 8.13\delta^{18}O + 11.93$	$\delta^2H = 5.43T - 114.19$	$\delta^{18}O = 0.67T - 15.49$

winter and lowest in the summer (increases of 0.73‰ $^{\circ}C^{-1}$ in the winter and 0.15‰ $^{\circ}C^{-1}$ in the summer). This characteristic determines the decrease of δ^2H–$\delta^{18}O$ slopes with SST increase (about 0.028 $^{\circ}C^{-1}$) (Table 4): the larger increment of d-excess values in the winter and smaller increment in the summer caused by increasing SST forces the δ^2H–$\delta^{18}O$ line to have a lower slope. When SST varies from 22 °C in the winter to 26 °C in the summer at the oceanic source region (fourth scenario), d-excess values reach their minima in *winter* and maximum in *summer*, compared with the first three scenarios, which corresponds with the highest δ^2H–$\delta^{18}O$ slope. The range of d-excess variation due to changes in SST is comparable to that from RH. For example, when SST = 22 °C, the d-excess at L_i changes from a winter value of 9.6‰ (RH over the source is 78%) to a summer value of 8.0‰ (RH over the source is 82%), whereas the d-excess value changes from 10.1‰ to 7.6‰ when the RH varies from 77% in the winter to 83% in the summer, or approximately 0.4‰ for every per cent change in RH.

5. Conclusions

This paper models the influence of vapour admixture from evaporation and transpiration as well as SST on the stable isotope compositions of hydrogen (δ^2H) and oxygen ($\delta^{18}O$) for continental condensates.

In a modified Rayleigh fractionation model (MRFM), two scenarios for evaporation and transpiration were proposed and their effects on the δ^2H and $\delta^{18}O$ values for condensates are described. The following conclusions were drawn:

(1) For the constant flux scenario, the input of evaporative vapour decreases the slopes of δ^2H–$\delta^{18}O$ and δ–T plots but increases the d-excess values. In contrast, the transpiration vapour exerts a minor effect on δ^2H–$\delta^{18}O$ slopes as well as d-excess values, but considerably reduces the δ–T slopes.

(2) For the stepwise flux scenario, evaporative vapour increases the δ^2H–$\delta^{18}O$ and decreases δ–T slopes as well as increases the d-excess values. In contrast, the transpiration vapour exerts minor effects on δ^2H–$\delta^{18}O$ slopes as well as the d-excess values, but considerably increases the δ–T slopes.

Thus, it is suggested that the isotope compositions of local condensates can be deduced from the MRFM once the evaporation and transpiration patterns are known. Moreover, the practical application of employing d-excess values to evaluate evaporation ratios and use of the slopes of δ–T curves to evaluate transpiration ratios appears feasible.

However, the proposed MRFM is still too simple because of numerous assumptions. It is not yet substantiated that this kind of inverse modelling can provide accurate answers about evaporation and transpiration ratios. This paper shows that the model is a self-consistent tool for understanding the isotope response of precipitation by evaporation and transpiration.

SST variation affects the isotope compositions of precipitation, regression equations as well as d-excess values. Although the influence of SST on the former are minor, the influence on d-excess is comparable to that from RH variation over the oceanic source. The result shows that seasonally varying SST significantly influences the d-excess and suggests that caution should be exercised in using d-excess and δ^2H and $\delta^{18}O$ versus T plots to interpret patterns in palaeotemperature proxies without also investigating other environmental parameters.

6. Appendix A: Symbols and Notation

C_D	Model-dependent "kinetic constant"
d_{adv}	d-excess value for advection water vapour
d_{evap}	d-excess value for evaporation water vapour
d_{surf}	d-excess value for surface water
e_i	Ratio of evaporation flux to precipitation flux at the segment $L_i(Fe/P_i)$
f	Fraction of vapour precipitated over the ocean
Fe	Evaporation flux at the segment L_i
f_e	Evaporation ratio
Ft	Transpiration flux at the segment L_i
f_t	Transpiration ratio
h_i	Relative humidity at segment L_i
h_o	Relative humidity above the ocean
L	Latent heat of evaporation
MRFM	Modified Rayleigh fractionation model
n	Factor depending on the wind regime over surface water
N_i	Flux of travelling vapour at the segment L_i
N_i°	Flux of travelling vapour at the segment L_{i+1}
N_V	Flux of travelling vapour
P_i	Precipitation flux at the segment L_i
R_E	Isotope composition for evaporation flux
R_i	Isotope composition for vapour in the atmosphere at the segment L_i
R_i'	Isotope composition for vapour in the atmosphere at the segment L_{i+1}
R_P	Isotope composition for precipitation
R_T	Isotope composition for transpiration water flux
R_w	Isotope composition for surface water
R_V	Isotope composition for the vapour in the atmosphere
$\overline{R_w}$	Long-term average value of isotope composition for local precipitation.
$\overline{R_{wi}}$	Long-term average value of isotope composition for precipitation at L_i
R_w'	Gas constant for vapour
T_E	Condensation temperature in the atmosphere
T_o	Sea surface temperature (SST)
t_i	Ratio of transpiration flux to precipitation flux at the segment $L_i(Ft/P_i)$
α_e	Isotope equilibrium fractionation factor of hydrogen or oxygen between liquid water and vapour
α^0	Kinetic fractionation factor during evaporation
θ	Weighting factor

References

Berner, E .K. and Berner, B. A. 1996. *Global Environment: Water, Air, and Geochemical Cycles*. Prentice Hall, Upper Saddle River, NJ, 10–50.

Chow, W. T. 1964. *Handbook of Applied Hydrology*. McGraw Hill, New York.

Craig, H. and Gordon, L. I. 1965. Deuterium and oxygen-18 variations in the ocean and the marine atmosphere. In: *Proceedings of the Conference on Stable Isotopes in Oceanographic Studies and Paleotemperatures* (ed. E. Tongiorgi). Laboratory of Geology and Nuclear Science, Pisa, 9–130.

Curry, J. A. and Webster, P. J. 1999. *Thermodynamics of Atmospheres and Oceans*. Academic Press, London, 168–179.

Dansgaard, W. 1964. Stable isotopes in precipitation. *Tellus* **16**, 436–468.

Gat, J. R., Bowser, C. J. and Kendall, C. 1994. The contribution of evaporation from the Great Lakes to the continental atmosphere, estimate based on stable isotope data. *Geophys. Res. Lett.* **21**, 557–560.

Gat, J. R. and Matsui, E. 1991. Atmospheric water balance in the Amazon Basin: an isotopic evapo-transpiration model. *J. Geophys. Res.* **96**, 13 179–13 188.

Hoffmann, G., Jouzel, J. and Masson, V. 2000. Stable water isotopes in atmospheric general circulation models. *Hydrol. Process.* **14**, 1385–1406.

Ingraham, N. L. and Taylor, B. E. 1991. Light stable isotope systematics of large-scale hydrologic regimes in California and Nevada. *Water Resour. Res.* **27**, 77–90.

Jacob, H. and Sonntag, C. 1991. An 8-year record of the seasonal variation of ^{2}H and ^{18}O in atmospheric water vapor and precipitation in Heidelberg, Germany. *Tellus* **43B**, 291–300.

Jouzel, J. and Merlivat, L. 1984. Deuterium and oxygen-18 in precipitation: modeling of the isotopic effect during snow formation. *J. Geophys. Res.* **89**, 11 749–11 757.

Letteu, H. 1954. A study of the mass momentum and energy budget of the atmosphere. *Arch. Meteorol., Geophys. Bioklimatol., Ser. A* **7**, 133–157.

Majoube, M. 1971. Fractionnement en oxygène-18 et en deutérium entre l'eau et sa vapeur. *J. Chem. Phys.* **197**, 1423–1436.

Merlivat, L. 1978. Molecular diffusivities of $H_2^{16}O$, $HD^{16}O$ and $H_2^{18}O$ in gases. *J. Chim. Phys.* **69**, 2864–2871.

Merlivat, L. and Jouzel, J. 1979. Global climatic interpretation of the deuterium–oxygen 18 relationship for precipitation. *J. Geophys. Res.* **84**, 5029–5033.

Moser, H. and Stichler, W. 1980. Environmental isotopes in ice and snow. In: *Handbook of Environmental Isotope Geochemistry* (eds. P. Fritz, and J. C. Fontes). Elsevier, Amsterdam, 141–178.

Peixoto, J. P. and Oort, A. H. 1983. The atmospheric branch of the hydrological cycle and climate. In: *Variations in the Global Water Budget* (eds A. Street-Perrott, M. Beran and R. Ratcliffe). Reidel, Dordrecht, 5–65.

Rozanski, K., Araguas-Araguas, L. and Gonfiantini, R. 1993. Isotopic pattern in modern global precipitation. In: *Climatic Change in Continental Isotopic Records*, American Geophysical Union Geophysical Monograph 78 (eds. P. K. Swart, K. L. Lohwan, J. Mckenzie and S. Savin). American Geophysical Union, Washington, DC, 1–37.

Salati, E., Dall'Olio, A., Matsui, E. and Gat, J. R. 1979. Recycling of water in the Amazon basin: an isotopic study. *Water Resour. Res.* **515**, 1250–1258.

Schotterer, U., Frohlich, K. and Stichler, W. 1993. Temporal variation of ^{18}O and deuterium excess in precipitation, river and spring water in alpine regions of Switzerland. In: *Isotope Techniques in the Study of Past and Current Environmental Changes in the Hydrosphere and the Atmosphere: Proceedings of a Symposium*, International Atomic Energy Agency, Vienna, 19–23.

Van der Straaten, C. M. and Mook, W. G. 1983. Stable isotope composition of precipitation and climatic variability. In: *Paleoclimate and Paleowaters: a Collection of Environmental Isotope Studies*. International Atomic Energy Agency, Vienna, 53–64.

Wang, X. F. and Yakir, D. 2000. Using stable isotopes of water in evapotranspiration studies. *Hydrol. Process.* **14**, 1407–1421.